Exciton dynamics in nanostar dendritic systems using a quantum master equation approach: Core monomer effects and possibility of energy transport control

ARTICLE *in* JOURNAL OF LUMINESCENCE · MARCH 2005

Impact Factor: 2.72 · DOI: 10.1016/j.jlumin.2004.10.016

5 AUTHORS, INCLUDING:

Masayoshi Nakano
Osaka University
337 PUBLICATIONS **4,793** CITATIONS
SEE PROFILE

Ryohei Kishi
Osaka University
110 PUBLICATIONS **1,955** CITATIONS
SEE PROFILE

Available online at www.sciencedirect.com
SCIENCE DIRECT®
Journal of Luminescence 111 (2005) 359–366
JOURNAL OF LUMINESCENCE
www.elsevier.com/locate/jlumin

Exciton dynamics in nanostar dendritic systems using a quantum master equation approach: core monomer effects and possibility of energy transport control

Masayoshi Nakano[a,*], Ryohei Kishi[a], Masahiro Takahata[b], Tomoshige Nitta[a], Kizashi Yamaguchi[b]

[a]*Department of Materials Engineering Science, Division of Chemical Engineering, Graduate School of Engineering Science, Osaka University, Toyonaka, Osaka 560-8531, Japan*
[b]*Department of Chemistry, Graduate School of Science, Osaka University, Toyonaka, Osaka 560-0043, Japan*

Available online 24 November 2004

Abstract

The directional energy transport, i.e. exciton migration, in nanostar dendritic systems composed of two-state monomer units is studied using a quantum master equation approach. We examine the effects of the variation in the excitation energy of the monomer in the core region (core monomer) on the multistep exciton migration from the periphery to the core based on the relaxation factors among exciton states originating in weak exciton–phonon coupling. It turns out that when the core monomer possesses both an excitation energy slightly lower than that of the first generation and a partial exciton overlap with the first generation, more efficient and rapid exciton migration to the core is expected as compared with other core monomer cases with the energy level closer to or much lower than that of the first generation.

PACS: 31.70.Hq; 36.40.Vz; 34.30.+h; 71.35.−y

Keywords: Nanostar; Energy transport; Exciton; Master equation; Relaxation

1. Introduction

Excitation energy transport is one of the essential processes in photosynthesis in green plants on earth and also finds an important application in photonics and biology [1–4]. Although typical energy transport is observed in

*Corresponding author. Tel.: +81 6 6850 6268; fax: +81 6 6850 6265.
E-mail address: mnaka@cheng.es.osaka-u.ac.jp (M. Nakano).

0022-2313/$ - see front matter © 2004 Elsevier B.V. All rights reserved.
doi:10.1016/j.jlumin.2004.10.016

supramolecular antenna involved in green plants and their artificial polymeric mimics, most of them have disordered structures in which energy transport is partially carried out by random walk, thermal activation and so on [5,6]. On the other hand, efficient and controllable energy transport is known to be one of the fascinating properties of dendrimers with ordered fractal-like architecture [7–16], which exhibits a directed, multistep energy transport of absorbed light. In particular, there have been lots of studies on the efficient light-harvesting properties of phenylacetylene dendrimers with a fractal-antenna (Cayley-tree) structure composed of many phenyl-ring and acetylene units [17–21]. It has been found that the efficient energy transport is carried out by the multistep exciton migration from the periphery to the core, and is related to two peculiar structural features: (I) increase in the lengths of linear legs involved in each generation as going from the periphery to the core and (II) *meta*-branching points (*meta*-substituted benzene rings). These features are predicted to provide multistep exciton states, in which the exciton distribution is spatially well localized in each generation from higher exciton states (distributed in the periphery region) to lower exciton states (distributed in the core region) [19,22–24]. In our previous studies using the dipole-coupled dendritic aggregate models [25–27], we have also pointed out the necessity of the relaxation effect between exciton states, originating in exciton–phonon coupling, for such efficient exciton migration in addition to multistep exciton states. The efficient multistep relaxation is found to require partial spatial overlaps of exciton distributions between neighboring exciton states, which are distributed in adjacent generations linked with *meta*-branching points. Our treatment has been extended and applied to real dendrimeric molecules based on *ab initio* molecular orbital (MO) configuration interaction (CI) calculations [28]. As a result, the structural features (I) and (II) are found to satisfy the following two conditions: (A) well-segmented exciton distribution in each multistep exciton state and (B) the existence of partial overlaps of exciton distributions between neighboring exciton states in order to realize efficient directed multistep exciton migration.

Similar to the Cayley-tree dendrimer, an associated dendrimer derivative, "nanostar", terminated at the focal point with a core monomer, e.g., a perylene luminophor, also exhibits efficient energy transport to the core monomer, which eventually emits the fluorescence enormously enhanced as compared to the case of an isolated core monomer [18–20,29]. In this paper, we investigate the effects of the variation in the excitation energy of core monomer on the exciton migration in the one-exciton dipole-coupled aggregate model with the nanostar structure. The quantum master equation approach including exciton–phonon coupling is applied. On the basis of the results, we discuss the relation between the coupling of the core monomer with the first generation in the nanostar and the feature of exciton migration in connection with the possibility of control of exciton migration by tuning the core monomer.

2. Methodology

Before investigating the exciton dynamics of the nanostar aggregate models, we briefly explain our calculation scheme [25–28] using a quantum master equation approach including exciton–phonon coupling. We consider a molecular aggregate composed of two-state monomers with excitation energies $\{E_i\}$ and magnitudes of transition dipole moments $\{\mu_i\}$ ($i = 1, 2, \ldots, N$, N: the number of monomers). The Hamiltonian, H_S, for the molecular aggregate is expressed by

$$H_S = \sum_i^N E_i |i\rangle\langle i| + \frac{1}{2}\sum_{i,j}^N J_{ij} |i\rangle\langle j|, \tag{1}$$

where $|i\rangle$ indicates the aggregate basis, which represents the situation that monomer i is excited. We assume a dipole–dipole intermolecular coupling between monomers i and j with an intermolecular distance R_{ij}:

$$J_{ij} = \frac{1}{4\pi\varepsilon_0 R_{ij}^3}\mu_i\mu_j\{\cos(\theta_{i_j} - \theta_{j_i}) - 3\cos\theta_{i_j}\cos\theta_{j_i}\}, \tag{2}$$

where θ_{i_j} (θ_{j_i}) is the angle between the transition moment of monomer $i(j)$ and the vector drawn from monomer i to j. The one-exciton states $\{|\psi_k\rangle\}$ with energies $\{\omega_k\}$ obtained by a diagonalization of H_S are expressed as

$$|\psi_k\rangle = \sum_i^N |i\rangle\langle i|\psi_k\rangle \equiv \sum_i^N C_{ki}|i\rangle \quad (k=2,\ldots,M), \tag{3}$$

where M is equal to $N+1$ for the one-exciton model and $k=1$ is reserved for the ground state of the system.

An exciton on monomer i is assumed to interact with a nuclear vibration, i.e. a phonon state $\{|q_i\rangle\}$ with a frequency $\{\Omega_{qi}\}$. The Hamiltonian, H_R, for the phonon is given by

$$H_R = \sum_i^N \sum_{q_i} \Omega_{q_i} c_{i,q_i}^+ c_{i,q_i}, \tag{4}$$

where c_{i,q_i}^+ and c_{i,q_i} represent the creation and annihilation operators concerning a phonon state $|q_i\rangle$, respectively. The interaction Hamiltonian, H_{SR}, for weak exciton–phonon coupling is assumed to be

$$H_{SR} = \sum_i^N \sum_{q_i} |i\rangle\langle i|(\kappa_{i,q_i}^* c_{i,q_i}^+ + \kappa_{i,q_i} c_{i,q_i}), \tag{5}$$

where κ_{i,q_i} denotes a coupling constant between an exciton on monomer i and a phonon state $|q_i\rangle$.

We focus on the dynamics of the exciton system involved in the total system composed of exciton (H_S), phonon (H_R) and their interaction (H_{SR}). Using the standard method of relaxation theory [30], we obtain a quantum master equation [26,27] for the exciton density matrix ρ under the Born–Markov approximation:

$$\dot{\rho}_{\alpha\alpha} = -\sum_m^M \Gamma_{\alpha\alpha;mm}\rho_{mm}, \tag{6}$$

and

$$\dot{\rho}_{\alpha\beta} = -i(\omega_\alpha - \omega_\beta)\rho_{\alpha\beta} - \sum_{m,n}^M \Gamma_{\alpha\beta;mn}\rho_{mn} \quad (\alpha \neq \beta). \tag{7}$$

The relaxation factors are expressed by

$$\Gamma_{\alpha\alpha;mm} = 2\delta_{\alpha m}\sum_k^M\sum_i^N |C_{\alpha i}|^2|C_{ki}|^2\gamma_{(i,i)}(\omega_m-\omega_k) - 2\sum_i^N |C_{\alpha i}|^2|C_{mi}|^2\gamma_{(i,i)}(\omega_m-\omega_\alpha) \tag{8}$$

and

$$\Gamma_{\alpha\beta;mn} = \sum_k^M\sum_i^N\big[\delta_{\beta n}C_{\alpha i}^*|C_{ki}|^2C_{mi}\gamma_{(i,i)}(\omega_m-\omega_k) + \delta_{\alpha m}C_{ni}^*|C_{ki}|^2C_{\beta i}\gamma_{(i,i)}(\omega_n-\omega_k)\big] - \sum_i^N\big[C_{\alpha i}^*C_{mi}C_{ni}^*C_{\beta i}\{\gamma_{(i,i)}(\omega_m-\omega_\alpha) + \gamma_{(i,i)}(\omega_n-\omega_\beta)\}\big], \tag{9}$$

where

$$\gamma_{(i,i)}(\omega) = \frac{2\gamma_{(i,i)}^0}{1+\exp(-\omega/k_BT)}. \tag{10}$$

This factor $\gamma_{(i,i)}(\omega)$ is taken to satisfy the thermal equilibrium condition [28,31]: $\gamma_{(i,i)}^0$ indicates the high-temperature limit of $\gamma_{(i,i)}(\omega)$, and k_B is the Boltzmann constant. We solve Eqs. (6) and (7) numerically using the fourth-order Runge–Kutta method.

In order to elucidate the relaxation pathway and relative relaxation rate, we employ a relative relaxation factor, $\Delta\gamma(\alpha\to\beta)$ [26,27]:

$$\Delta\gamma(\alpha\to\beta) = 2\sum_i^N |C_{\alpha i}|^2\big|C_{\beta i}\big|^2\{\gamma_{(i,i)}(\omega_\alpha-\omega_\beta) - \gamma_{(i,i)}(\omega_\beta-\omega_\alpha)\}, \tag{11}$$

where the first and second terms on the right-hand side represent the transition rate from state α to β and that from state β to α, respectively. The direction and the magnitude of exciton relaxation between exciton states are represented by the sign and the absolute value of $\Delta\gamma(\alpha\to\beta)$, respectively: positive (negative) $\Delta\gamma(\alpha\to\beta)$ indicates the relaxation from state α (β) to $\beta(\alpha)$. The terms in wavy parenthesis in Eq. (11) relate to the energy difference between exciton states α and β, whereas $|C_{\alpha i}|^2|C_{\beta i}|^2$ in Eq. (11) corresponds to the overlap of exciton distributions in site i between the two exciton states α and β. This implies that an overlap

between the distributions of two exciton states is indispensable for non-zero $\Delta\gamma(\alpha\rightarrow\beta)$, i.e., relaxation from state α to β.

3. Results and discussion

3.1. Exciton states of N23

We consider a nanostar dentritic aggregate, N23, composed of 22 two-state monomers ($38000\,cm^{-1}$ and 10 D) and three types of core monomers (models **c1** ($35000\,cm^{-1}$, 10 D), **c2** ($34000\,cm^{-1}$, 10 D) and **c3** ($32000\,cm^{-1}$, 10 D)) which terminate a focal point of the nanostar (see Fig. 1). The aggregate model N23 satisfies the two structural features mentioned in Section 1. Dipole–dipole coupling is assumed among all pairs of monomers in the whole region. Feature (I) is realized by increasing the number of *J*-aggregate-type monomers involved in the linear-leg regions as going from the periphery to the core, whereas feature (II) is realized by the fact that the intermolecular distances ($10\sqrt{3}$ a.u.) between the adjacent legs at the branching points are larger than those in the linear-leg regions (10 a.u.).

Fig. 2 shows the excitation energies and transition moments between the ground (**1**) and the one-exciton states ($\geqslant$**2**) obtained by diagonalizing the coupled-dipole Hamiltonian (Eq. (1)). As a result, there are multistep exciton states with and without

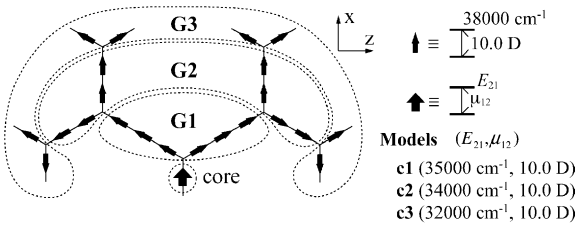

Fig. 1. Structure of the nanostar dendritic molecular aggregate, N23, in which all the units except for the core are composed of two-state monomers (expressed by arrows) with excitation energy, $38000\,cm^{-1}$ and transition moment, 10 D. Three types of core monomers, **c1** ($35000\,cm^{-1}$, 10 D), **c2** ($34000\,cm^{-1}$, 10 D) and **c3** ($32000\,cm^{-1}$, 10 D), are considered. The intermolecular distance in linear legs is fixed to be 10 a.u. Symbols **G1**, **G2** and **G3** depict the first, second and third generations of the nanostar, and the core is represented by a thick arrow.

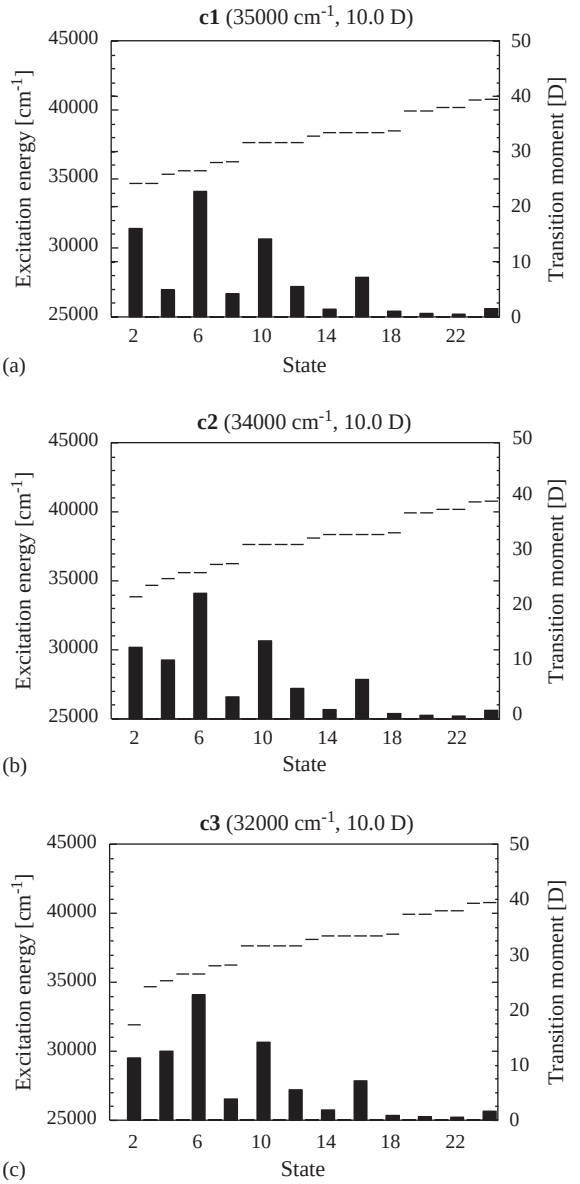

Fig. 2. Excitation energies, *E*, and the magnitude of transition moments, μ, between the ground and one-exciton states for models **c1**–**c3**.

transition moments from the ground state. All models show almost the same energy-level structures of multistep exciton states beyond state **4**. States **10** ($37659\,cm^{-1}$, 14.1 D) and **9** ($37646\,cm^{-1}$, 0 D) have the exciton distribution in **G3**, states **8** ($36258\,cm^{-1}$, 3.8 D) and **7** ($36215\,cm^{-1}$, 0 D) have

the exciton distribution in outer parts in **G2**, and states **6** (35632 cm^{-1}, 22.7 D) and **5** (35622 cm^{-1}, 0 D) have the exciton distribution in inner parts in **G2**. On the other hand, the exciton energies and distributions of states **4**, **3** and **2** are changed depending on the excitation energies of the core monomers in these models. For model **c1** (35000 cm^{-1}, 10 D), state **3** (34722 cm^{-1}, 0 D) has the main exciton distribution in **G1** (95%), whereas states **4** (35365 cm^{-1}, 4.9 D) and **2** (34705 cm^{-1}, 16.0 D) have the main distributions in two generations: **G1** (54% for state **4** and 37% for state **2**) and core (37% for state **4** and 61% for state **2**). In contrast, for model **c2** (34000 cm^{-1}, 10 D), states **4** (35200 cm^{-1}, 10.7 D) and **3** (34722 cm^{-1}, 0 D) have the main exciton distributions in **G1** (84% and 95%, respectively), while the lowest exciton state **2** (33883 cm^{-1}, 13.0 D) has the main distribution in the core (93%). For model **c3** (32000 cm^{-1}, 10 D), states **4** (35149 cm^{-1}, 12.5 D) and **3** (34722 cm^{-1}, 0 D) have the main exciton distributions in **G1** (90% and 95%, respectively) similar to model **c2**, while the energy of the lowest exciton state **2** (31945 cm^{-1}, 11.3 D) with the main distribution in the core (99%) is significantly lower than that of model **c2**. As a result, the gradient of exciton energy in the lowest exciton states **4**, **3** and **2** increases while going from model **c1** to **c3**. It is also noted that the energy difference between **G1**, in which the exciton in state **4** is primarily distributed for models **c2** and **c3**, and the core monomer (35000 cm^{-1}, 10 D) is smaller for model **c1** than that for the other models, so that both states **4** and **2** for model **c1** involve significant exciton distributions in the core due to the strong coupling between the core monomer and **G1**. This suggests that model **c1** exhibits an incomplete concentration of the exciton to the core, which is reflected in the relatively low population (61%) in the core in the lowest exciton state **2**.

3.2. Exciton migration dynamics of N23

The exciton dynamics of N23 is performed using Eqs. (6)–(10) with the initial population in state **10**, which has the main exciton distribution in the periphery region (**G3**) and has a large transition moment (14.1 D) from the ground state for these models. Such dynamics is sufficient for our purpose of clarifying the exciton migration (relaxation) pathways for models **c1–c3** and their efficiency though in real experiments the exciton is firstly generated primarily in state **10** by applying a laser field with a resonant frequency to state **10**. The high-temperature limit value $\gamma^0_{(i,i)}$ (see Eq. (10)) for all monomers and the temperature T are assumed to be 200 cm^{-1} and 300 K, respectively. It is noted that these parameters do not influence the qualitative features of relaxation pathways and relative relaxation rates but only affect the absolute values of relaxation rates. Fig. 3 shows the time evolution of the exciton distributions in each region, **G3**, **G2**, **G1** and core, for 32000 time steps, in which a time step corresponds to about 0.1 fs. For all models, we observe the decrease of the exciton population in **G3** and the subsequent increase of exciton population in **G2**, which takes a maximum at around 4000 steps and then decreases. The variation of the exciton population between **G1** and the core is significantly different among these models: models **c2** (34000 cm^{-1}, 10 D) and **c3** (32000 cm^{-1}, 10 D) exhibit the concentration of exciton population in the core following the increase of population in **G1**, whereas for model **c1** (35000 cm^{-1}, 10 D), the exciton population in the core increases at the same rate with that in **G1** and does not overcome that in **G1** but converges to the distribution ratio, **G1**: core = 37: 61, which is the exciton distribution in the lowest exciton state **2**. It is also found from the comparison of model **c2** with **c3** that the increase of the exciton population in the core for model **c3** is much slower than that for model **c2** though the energy gradient for the lowest three exciton states is steeper for model **c3** than for model **c2** (see Fig. 2). This feature causes the distinct increase behavior of the population in **G1** for model **c3** as compared to model **c2**. As pointed out in our previous paper [25–28], in order to understand this difference in exciton migration, we have to remember the importance of not only the energy gradient of multistep exciton states but also the relaxation between exciton states depending on their exciton overlap (see Eq. (8)). In the next section, the relation between the exciton distribution and the main relaxation pathway is elucidated for models **c1–c3** as well as their relative

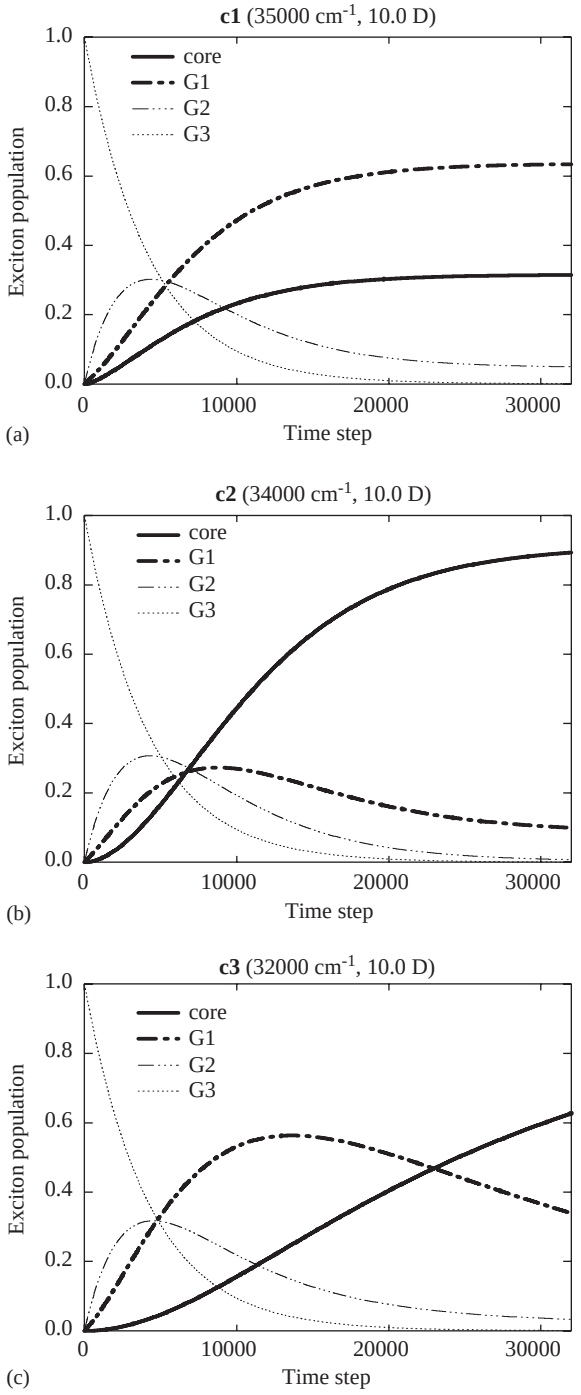

Fig. 3. Variation in exciton populations of core, **G1**–**G3** for N23. State **10** is initially populated and has the dominant exciton distribution in **G3**. A time step corresponds to about 0.1 fs.

relaxation rates using relative relaxation factors (Eq. (11)).

3.3. Analysis of exciton migration pathways of N23

Fig. 4 shows the primary exciton relaxation (migration) pathways with dominant relative relaxation factors $\Delta\gamma(\alpha\rightarrow\beta)$ for models **c1**–**c3** of N23. The values in parentheses represent the energy-dependent term, i.e., the sum of values in

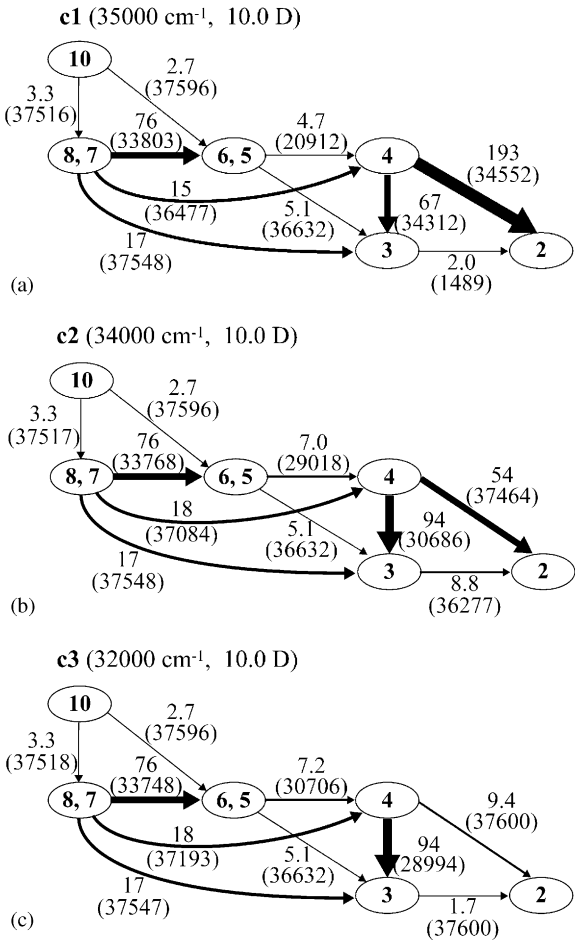

Fig. 4. Relative relaxation factors $\Delta\gamma(\alpha\rightarrow\beta)$ (cm^{-1}) (Eq. (11)) between exciton states for N23. The numbers in circles and the arrows represent the exciton states and the direction of exciton relaxation, respectively. The numbers in parentheses are the values of $2\sum_i^N\{\gamma_{(i,i)}(\omega_\alpha-\omega_\beta)-\gamma_{(i,i)}(\omega_\beta-\omega_\alpha)\}$ in Eq. (11). They are the averaged values of relaxation factors among exciton states in circles connected by arrows. Thicker lines represent faster relaxation pathways.

wavy parenthesis in Eq. (11). The exciton overlap represented by $|C_{\alpha i}|^2|C_{\beta i}|^2$ is found to significantly reduce the magnitude of energy-dependent terms in the relaxation factor and changes the relative intensity. It turns out for all models that the primary exciton pathways are almost the same from state **10** to states **3** and **4** (**G1**), whereas the relative relaxation factors for the pathways among states **4**, **3** and **2** are remarkably different from each other for these models. For models **c1** and **c2**, the relaxations from state **4** to states **2** and **3** ($\Delta\gamma(\mathbf{4}\rightarrow\mathbf{2}) = 193\,\mathrm{cm}^{-1}$ and $\Delta\gamma(\mathbf{4}\rightarrow\mathbf{3}) = 67\,\mathrm{cm}^{-1}$ for model **c1**, $\Delta\gamma(\mathbf{4}\rightarrow\mathbf{2}) = 54\,\mathrm{cm}^{-1}$ and $\Delta\gamma(\mathbf{4}\rightarrow\mathbf{3}) = 94\,\mathrm{cm}^{-1}$ for model **c2**) are much faster than those from state **3** to **2** ($\Delta\gamma(\mathbf{3}\rightarrow\mathbf{2}) = 2.0\,\mathrm{cm}^{-1}$ for model **c1**, $\Delta\gamma(\mathbf{3}\rightarrow\mathbf{2}) = 8.8\,\mathrm{cm}^{-1}$ for model **c2**), whereas for model **c3**, both pathways, **4**→**2** and **3**→**2**, have the smallest relaxation factors ($\Delta\gamma(\mathbf{4}\rightarrow\mathbf{2}) = 9.4\,\mathrm{cm}^{-1}$ and $\Delta\gamma(\mathbf{3}\rightarrow\mathbf{2}) = 1.7\,\mathrm{cm}^{-1}$) in the same pathways in these models. For model **c1**, the relaxation from state **4** to **2** is about three times as fast as that from state **4** to **3**, while for model **c2**, the relaxation from state **4** to **3** is about twice as fast as that from state **4** to **2**. These features are understood by the difference in exciton overlap among states **4**, **3** and **2** for these models (see Fig. 5). From Eq. (11), $\Delta\gamma(\alpha\rightarrow\beta)$ becomes large in the case of large exciton overlap between exciton states. For model **c1**, since both states **4** and **2** have significant exciton distributions in the core due to the strong coupling between these two states, $\Delta\gamma(\mathbf{4}\rightarrow\mathbf{2})$ takes a large value. On the other hand, for model **c2**, states **4** and **3** have similar exciton distributions in **G1**, while the exciton overlap between states **2** and **4**, which corresponds to that between **G1** and core, is smaller than that for model **c1**: this feature corresponds to the difference in the relaxation feature between model **c1** and **c2** (see Figs. 3 and 4). Contrary to models **c1** and **c2**, model **c3** has no significant relaxation pathways from states **4** and **3** to state **2** (see Fig. 4(c)), which is found to be caused by the disappearance of the exciton overlap between state **4** (**3**) and state **2** (see Fig. 5(c)) due to the large energy difference between the core monomer ($32000\,\mathrm{cm}^{-1}$) and states **4** and **3** ($\approx 35000\,\mathrm{cm}^{-1}$). It is therefore found that although the exciton population for model **c3** is concentrated in the core eventually in contrast to model **c1**, it takes a longer time to achieve a concentration of exciton in the core than in the case of model **c2**.

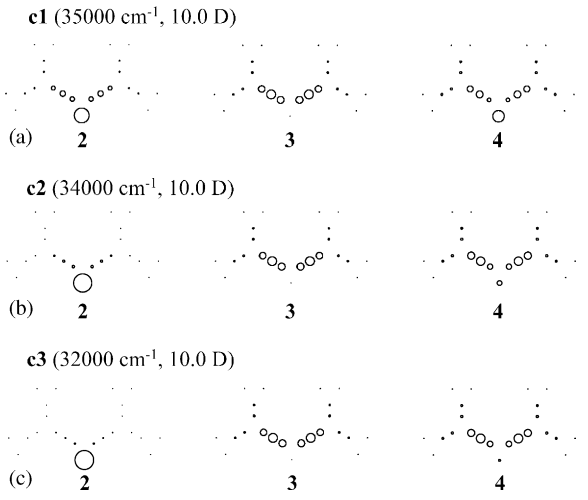

Fig. 5. Exciton spatial distributions (the squares of exciton wave functions) of low-lying exciton states **4**, **3** and **2** for N23. The circle represents the size of exciton distribution at the position of each monomer.

4. Concluding remarks

Using the quantum master equation approach, we have investigated the effect of changing the excitation energy of the core monomer on the exciton migration for the nanostar dendritic aggregates modeled after the nanostar dendrimers. It is found that the nanostar dendritic aggregate, which involves the core monomer with the energy slightly lower than that of the exciton state with the main distribution in the first generation, shows an efficient and rapid exciton migration (energy transport) from the periphery to the core similar to the Cayley-tree dendritic systems. On the other hand, it turns out that when the core monomer possesses an excitation energy close to that of the exciton state of the first generation, we cannot observe the complete exciton concentration in the core since both the lowest exciton state, into which the exciton finally relaxes, and the slightly higher-lying exciton state involving the distribution in the first generation have significant exciton distribu-

tions in the core region. Furthermore, although the core monomer with an too large energy difference from the exciton state involving the primary distribution in the first generation gives a large energy gradient, it does not exhibit a rapid exciton migration from the periphery to the core since the exciton overlap between the core monomer and the first generation is almost negligible.

In conclusion, the feature of multistep exciton migration from the periphery to the core in the nanostar dendritic systems is predicted to be sensitively influenced by the degree of coupling between the core and the first generation. The most effective and rapid exciton migration to the core is expected to be realized in the intermediate coupling regime between the core and the first generation in the nanostar system with an energy funnel. For example, the tuning of energy and transition moment of the core by chemical modification to satisfy this condition will lead to an optimal control of the efficiency and speed of exciton migration.

Acknowledgments

This work was supported by Grant-in-Aid for Scientific Research (No. 14340184) from the Japan Society for the Promotion of Science (JSPS).

References

[1] R.S. Knox, in: J. Barber (Ed.), Primary Processes of Photosynthesis, vol. 2, Elsevier, Amsterdam, 1977.
[2] B. Deming-Adams, Biochim. Biophys. Acta 1020 (1990) 1.
[3] L. Valkunas, N.E. Geacintov, L.L. France, J. Lumin. 51 (1992) 67.
[4] A. Archut, G.C. Azzellini, V. Balzani, L. De Cola, F. Vögtle, J. Am. Chem. Soc. 120 (1998) 12187.
[5] A.H. Francis, R. Kopelman, in: W.M. Yen, P.M. Selzer (Eds.), Laser Spectroscopy of Solids, Springer, Berlin, 1986, p. 241.
[6] O.J.G. Somsen, F.v. Mourik, R.v. Grondel, L. Valkunas, J. Biophys. 66 (1994) 1.
[7] E. Buhleier, W. Wehner, F. Vögtle, Synthesis (1978) 155.
[8] C. Hawker, J.M.J. Fréchet, J. Am. Chem. Soc. 112 (1990) 7638.
[9] J.M.J. Fréchet, Science 263 (1994) 1710.
[10] M. Fischer, F. Vögtle, Angew. Chem. Int. Ed. 38 (1999) 884.
[11] A.W. Bosman, H.M. Janssen, E.W. Meijer, Chem. Rev. 99 (1999) 1665.
[12] D.N. Reinhoudt (Ed.), Supramolecular Materials and Technologies, Perspectives in Supramolecular Chemistry, vol. 4, Wiley, New York, 1999.
[13] M. Nakano, K. Yamaguchi, Advances in Multi-photon Processes and Spectroscopy, vol. 15, World Scientific, Singapore, 2003, p. 1.
[14] M. Nakano, H. Fujita, M. Takahata, K. Yamaguchi, J. Am. Chem. Soc. 124 (2002) 9648.
[15] M. Nakano, H. Fujita, M. Takahata, K. Yamaguchi, J. Chem. Phys. 115 (2001) 1052.
[16] M. Nakano, H. Fujita, M. Takahata, K. Yamaguchi, J. Chem. Phys. 115 (2001) 6780.
[17] Z. Xu, J.S. Moor, Acta Polym. 45 (1994) 83.
[18] C. Devadoss, P. Bharathi, J.S. Moore, J. Am. Chem. Soc. 118 (1996) 9635.
[19] M.R. Shortreed, S.F. Swallen, Z.-Y. Shi, W. Tan, Z. Xu, C. Devadoss, J.S. Moore, R. Kopelman, J. Phys. Chem. B 101 (1997) 6318.
[20] R. Kopelman, M. Shortreed, Z.-Y. Shi, W. Tan, A. Bar-Haim, J. Klafter, Phys. Rev. Lett. 78 (1997) 1239.
[21] A. Bar-Haim, J. Klafter, R. Kopelman, J. Am. Chem. Soc. 26 (1997) 6197.
[22] S. Tretiak, V. Chernyak, S. Mukamel, J. Phys. Chem. B 102 (1998) 3310.
[23] J.C. Kirkwood, C. Scheurer, V. Chernyak, S. Mukamel, J. Chem. Phys. 114 (2001) 2419.
[24] S. Tretiak, S. Mukamel, Chem. Rev. 102 (2002) 3171.
[25] M. Nakano, M. Takahata, H. Fujita, S. Kiribayashi, K. Yamaguchi, Chem. Phys. Lett. 323 (2000) 249.
[26] M. Takahata, M. Nakano, H. Fujita, K. Yamaguchi, Chem. Phys. Lett. 363 (2002) 422.
[27] M. Takahata, M. Nakano, K. Yamaguchi, J. Theor. Comput. Chem. 2 (2003) 459.
[28] M. Nakano, M. Takahata, S. Yamada, K. Yamaguchi, R. Kishi, T. Nitta, J. Chem. Phys. 120 (2004) 2359.
[29] V.D. Kleinman, J.S. Melinger, D.J. McMorrow, J. Phys. Chem. B 105 (2001) 5595.
[30] H.J. Carmichael, Statistical Methods in Quantum Optics 1, Springer, Berlin, 1999.
[31] J.A. Leegwater, J.R. Durrant, D.R. Klug, J. Phys. Chem. B 101 (1997) 7205.